

Article

Not peer-reviewed version

Bacterial Cellulose from Kombucha Pellicle for Mucoadhesive Nanoformulations – A Comparison with Vegetal Cellulose from Brewer's Spent Grains

Ioana Popa Tudor , [Naomi Tritean](#) , [Ștefan-Ovidiu Dima](#) , [Bogdan Trică](#) , [Marius Ghiurea](#) , [Anisoara Cimpean](#) , [Florin Oancea](#) ^{*} , [Diana Constantinescu-Aruxandei](#) ^{*}

Posted Date: 4 December 2024

doi: 10.20944/preprints202412.0335.v1

Keywords: nanocellulose; brewer's spent grains; Kombucha fermentation; hydrogels; cytocompatibility; gingival fibroblasts; mucoadhesion



Preprints.org is a free multidisciplinary platform providing preprint service that is dedicated to making early versions of research outputs permanently available and citable. Preprints posted at Preprints.org appear in Web of Science, Crossref, Google Scholar, Scilit, Europe PMC.

Copyright: This open access article is published under a Creative Commons CC BY 4.0 license, which permit the free download, distribution, and reuse, provided that the author and preprint are cited in any reuse.

Article

Bacterial Cellulose from Kombucha Pellicle for Mucoadhesive Nanoformulations – A Comparison with Vegetal Cellulose from Brewer's Spent Grains

Ioana Popa-Tudor ^{1,‡}, Naomi Tritean ^{1,2,‡}, Ștefan-Ovidiu Dima ¹, Bogdan Trică ¹,
Marius Ghiurea ¹, Anisoara Cimpean ², Florin Oancea ^{1,*} and Diana Constantinescu-Aruxandei ^{1,*}

¹ Polymers and Bioresources Departments, National Institute for Research and Development in Chemistry and Petrochemistry – ICECHIM, Splaiul Independentei nr. 202, sector 6, 060021 Bucharest, Romania

² Faculty of Biology, University of Bucharest, Splaiul Independentei nr. 91-95, 050095 sector 5, Bucharest, Romania

* Correspondence: diana.constantinescu@icechim.ro; florin.oancea@icechim.ro; Tel.: +40 21 315 3299

‡ These authors contributed equally

Abstract: Cellulose nanofibers have gained increasing interest in the production of medical devices such as mucoadhesive nanohydrogels due to their ability to retain moisture (high hydrophilicity), flexibility, superior porosity and durability, biodegradability, non-toxicity, and biocompatibility. In this work we aimed to compare the suitability of bacterial and vegetal nanocellulose to form hydrogels for biomedical applications. Therefore, vegetal and bacterial cellulose nanofibers were synthesized from brewer's spent grains (BSG) and Kombucha membranes, respectively. Two hydrogels were prepared, one based on the vegetal and the other based on the bacterial cellulose nanofibers (VNC and BNC, respectively). The two hydrogels, as well as the hydrogel-mucin systems were physicochemically characterized. The cytocompatibility of the nanocellulose-based hydrogels was investigated using human gingival fibroblasts (HGF-1, ATCC CRL-2014). The morphological analyses highlighted the similarities and differences between bacterial and vegetal nanocellulose. The investigation of the hydrogel-mucin interaction revealed that the BNC hydrogel has a higher mucin binding efficiency than the VNC hydrogel. The BNC hydrogel exhibited the highest potential to increase the number of metabolically active viable cells ($107.60 \pm 0.98\%$ of cytotoxicity negative control). The data suggest that the BNC hydrogel based on nanocellulose from Kombucha fermentation could be a better candidate for cytocompatible and mucoadhesive nanoformulations than the VNC hydrogel based on nanocellulose from brewer's spent grains.

Keywords: nanocellulose; brewer's spent grains; Kombucha fermentation; hydrogels; cytocompatibility; gingival fibroblasts; mucoadhesion

1. Introduction

The study of polymers with mucoadhesive properties began in 1947 with the attempts of Scrivener and Schantz to develop an effective formulation for the delivery of penicillin [1]. Subsequently, several delivery systems were developed, e.g., hydrogels, emulsions, suspensions, films, tablets, capsules, patches etc. Mucoadhesion is a particular physicochemical phenomenon of bioadhesion, in which the process of interfacial adsorption-adhesion takes place on a mucilaginous surface [2]. The term derives from a class of natural glycoproteins – mucins, which are produced by the epithelial tissue, being present in the areas lined by the epithelial mucosa (oral, vaginal, nasal, intestinal etc.) and having the defining property of increased protection and lubrication [3]. The mucoadhesion of different formulations is studied in relation to different mucosal tissues to ensure a targeted and optimal release of encapsulated active substances. Moreover, the adhesion of

transdermal patches or dressings for various health conditions is of interest in the biomedical field [4]. The treatment of the oral mucosal conditions requires a long-term adherence of the therapeutic agent to the target site. The adhesion may be hindered by the continuous salivary flow or the mechanical movements of the tongue. Therefore, the formulations that act as a vehicle for the delivery of different bioactive compounds/drugs to the oral mucosa must exhibit excellent mucoadhesive properties [5,6].

Mucoadhesive properties have been discovered and exploited for several oligo- and polysaccharides, proteins and peptides. Among the most studied polymers with mucoadhesive properties used as mucosal delivery systems are cellulose, hyaluronic acid, alginate, chitosan, carbomers and their derivatives [7,8]. Cellulose is an abundant natural polymer composed of D-glucopyranose units linked by β -1, 4-glycosidic bonds [9]. It is well known that the lignocellulosic matrices are a valuable source of cellulose. Although vegetal cellulose is nature's most abundant biopolymer, it is difficult to obtain nanocellulose from complex vegetal matrices where it is combined with hemicellulose, pectin and lignin in order to form the plant cell wall. As a result, the production of cellulose by bacteria and microbial fermentative processes, e.g., using a Symbiotic Culture of Bacteria and Yeasts (SCOBY) such as the one from Kombucha, has gained a great interest. This is due to the specific physicochemical properties that result from the biosynthesis process and that influence the biological activities.

Vegetal and bacterial nanocellulose represent promising biopolymers for the biomedical field due to their biocompatibility, hydrophilic nature, biodegradability, non-toxicity [10], water retention capacity [11,12], superior flexibility and porosity, increased durability [13]. Due to the macromolecular chains that present a high number of -OH and -COOH functional groups which are responsible for the ability of nanocellulose to adsorb and retain water, it can form hydrogels by establishing new inter-chain hydrogen bonds. The structure of hydrogels can be irreversible in the presence of certain cross-linking agents or reversible through physicochemical interactions [7]. Reversible hydrogels have been shown to exhibit superior mucoadhesive properties than irreversible hydrogels due to the high mobility of the chains. A suitable hydrogel for biomedical applications should exhibit a sol-gel transition under specific conditions without releasing toxic byproducts or having a negative impact on the surrounding tissues [14]. The cells can also be incorporated into the hydrogels creating 3D cellular scaffolds that lead to tissue regeneration [15,16].

Bacterial (nano)cellulose was shown to have some distinct properties compared with the vegetal (nano)cellulose, such as higher purity, higher crystallinity, mechanical stability, higher water-holding capacity, and less-intensive purification processes than plant (nano)cellulose [17–22]. Plant (nano)cellulose has the advantage of antimicrobial, antioxidant and anti-inflammatory properties compared to bacterial (nano)cellulose [18–20]. It is generally considered that bacterial (nano)cellulose is more suitable for biomedical applications, but there are limited studies to directly compare bacterial (nano)cellulose with vegetal (nano)cellulose for biomedical applications under the same conditions. In a study from 2013 bacterial cellulose was tested for dental canal treatment and proven to be superior to paper points (plant cellulose), which is a conventional material [23].

In the light of the above, the aim of this study was to compare the capacity of selected bacterial and vegetal nanocellulose to form mucoadhesive and cytocompatible hydrogels. Two types of cellulose nanofiber-based hydrogels, respectively a hydrogel based on vegetal nanocellulose from brewer's spent grains (VNC) and a hydrogel based on bacterial nanocellulose from Kombucha fermentation (BNC) were compared. Brewer's spent grains (BSG) represent a lignocellulosic by-product from the beer industry that can be exploited for the recovery of cellulose, lignin, carbohydrates, glycoproteins, polyphenols [24]. We selected BSG as it is one of the most abundant lignocellulosic by-products and which can be collected from a concentrated source [25]. Kombucha is a known fermented, sweetened black tea that produces a thick bacterial cellulose membrane as a by-product, which represents a more cost-effective source of bacterial cellulose. By recycling the residual materials, value-added biocompounds /biomaterials can be obtained for several applications, i.e., biotechnological or pharmacological products, medical devices etc. [26]. Physicochemical properties, hydrogel-mucin interaction and the resulting complexes (VNCMu and

BNCMu, respectively) and the cytocompatible behavior were characterized in order to assess the hydrogels as potential candidates for various biomedical applications.

2. Results and Discussion

2.1. Physicochemical Properties of Nanocellulose-Based Hydrogels and Hydrogel-Mucin Systems

A schematic representation of the main steps involved in the preparation of the two nanohydrogels (VNC and BNC) is depicted in Figure 1. As can be seen both types of cellulose have a whitish appearance which indicates high purity upon purification. The hydrogels have a translucent and similar appearance.

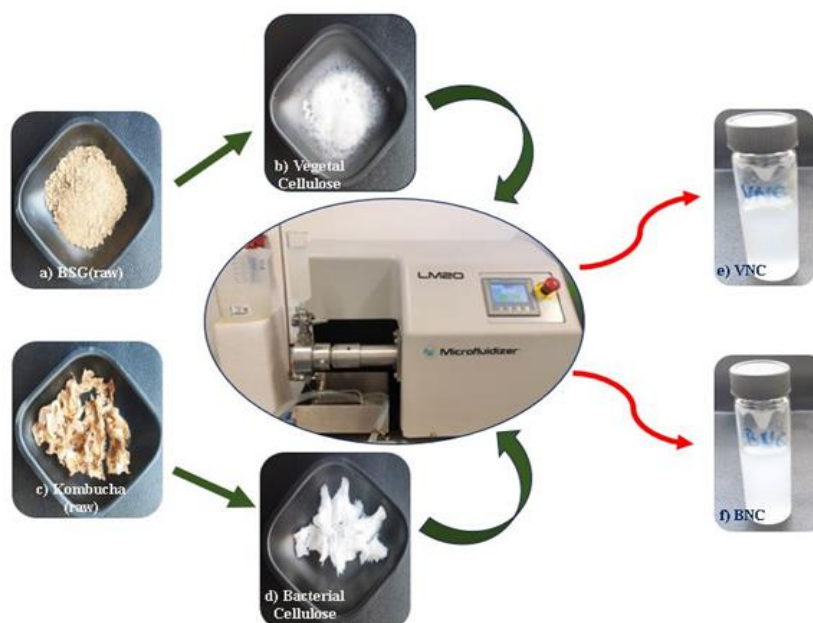


Figure 1. Schematic representation of cellulose purification and hydrogel preparation: (a) Brewer's spent grains (BSG); (b) Purified vegetal cellulose from BSG; (c) Bacterial cellulose (BC) membrane from Kombucha fermentation; (d) Purified BC; (e) Hydrogel of vegetal nanocellulose from BSG (VNC); (f) Hydrogel of bacterial nanocellulose from Kombucha fermentation (BNC).

TEM analysis highlighted the nanofibrillar structure of the two types of nanocellulose-based hydrogels. The nanofibers of the VNC hydrogel are a little shorter and rarer (Figure 2a,b) in comparison with the nanofibers of the BNC hydrogel, which interweave into a dense network-like structure (Figure 2c,d). The type of biomass can lead to significant differences in the structure of nanocellulose. Cellulose nanofibers from poplar wood exhibited larger diameters than those from rice straw and a looser arrangement, as revealed by TEM analysis [27]. In our previously reported study, by bleaching of bacterial cellulose with sodium hydroxide followed by colloidal mill grinding and 25 cycles of microfluidization, TEM analysis revealed the formation of a uniform mesh-like structure, with the diameter of the cellulose nanofibrils being about 10-50 nm. By using the spray-drying process instead of microfluidization, fibrillar bundle or ribbon-like structures of nanocellulose were obtained [28], suggesting the development of different cellulosic nanostructures based on the mechanical deconstruction technique.

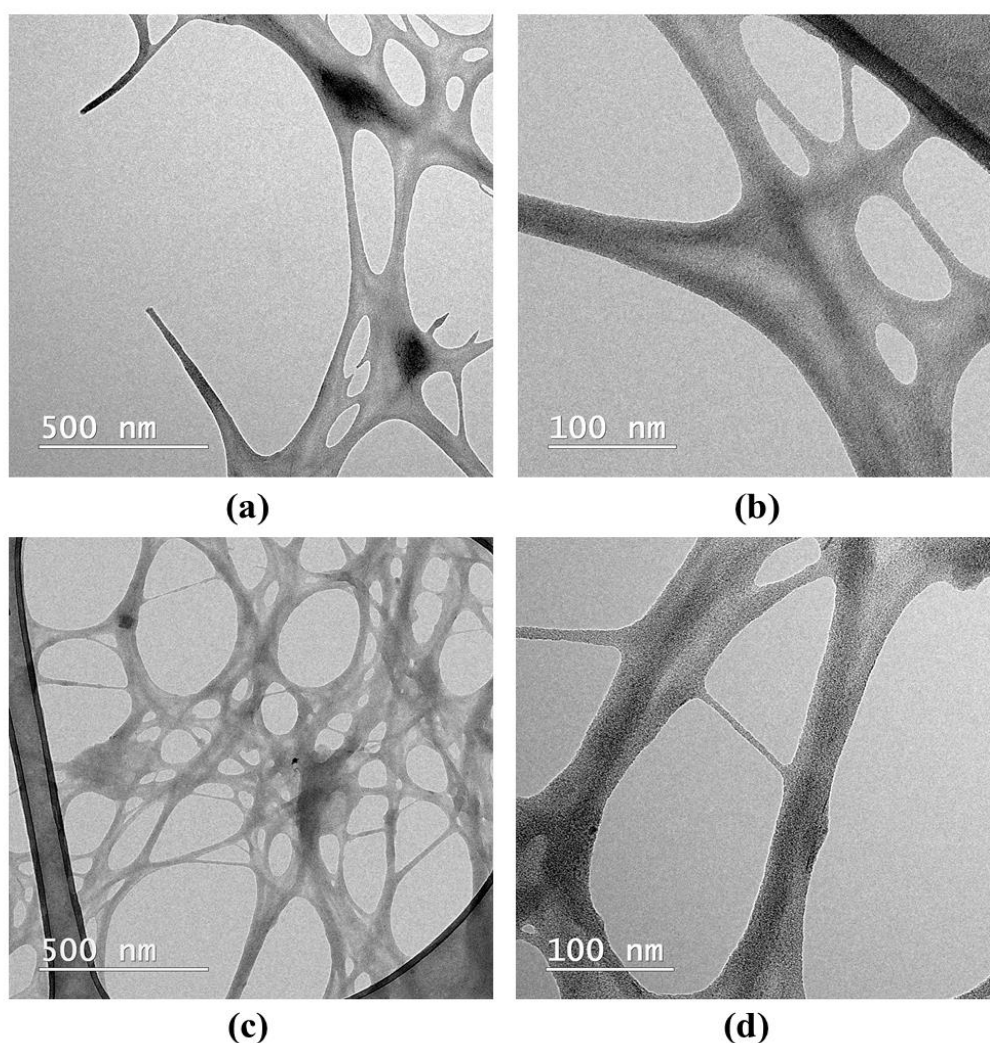


Figure 2. TEM analysis of: (a) VNC (500 nm scale), (b) VNC (100 nm scale); (c) BNC (500 nm scale); (d) BNC (100 nm scale); VNC – hydrogel of vegetal nanocellulose from brewer's spent grains; BNC – hydrogel of bacterial nanocellulose from Kombucha fermentation.

The SEM analyses of VNC and BNC hydrogels highlighted some differences in the structure and the arrangement of the two types of cellulose nanofibers. The secondary electrons (SE) detector was used in order to investigate the topography of the samples (Figure 3), and the backscattered electrons (BSE) detector provided structural insights from a larger depth (Figure 4). From SEM analysis using the SE detector, some brighter areas were observed which might correspond to an electron dense structure most likely attributed to the crystalline microstructure of cellulose. The darker areas are correlated with a less dense structure and most likely attributed to the coarser and disordered structure of amorphous cellulose (Figure 3). The VNC hydrogel exhibited a more relaxed arrangement of cellulose fibers (Figures 3a and 4a) in comparison with the mesh-like structure of BNC (Figure 3b, 4b).

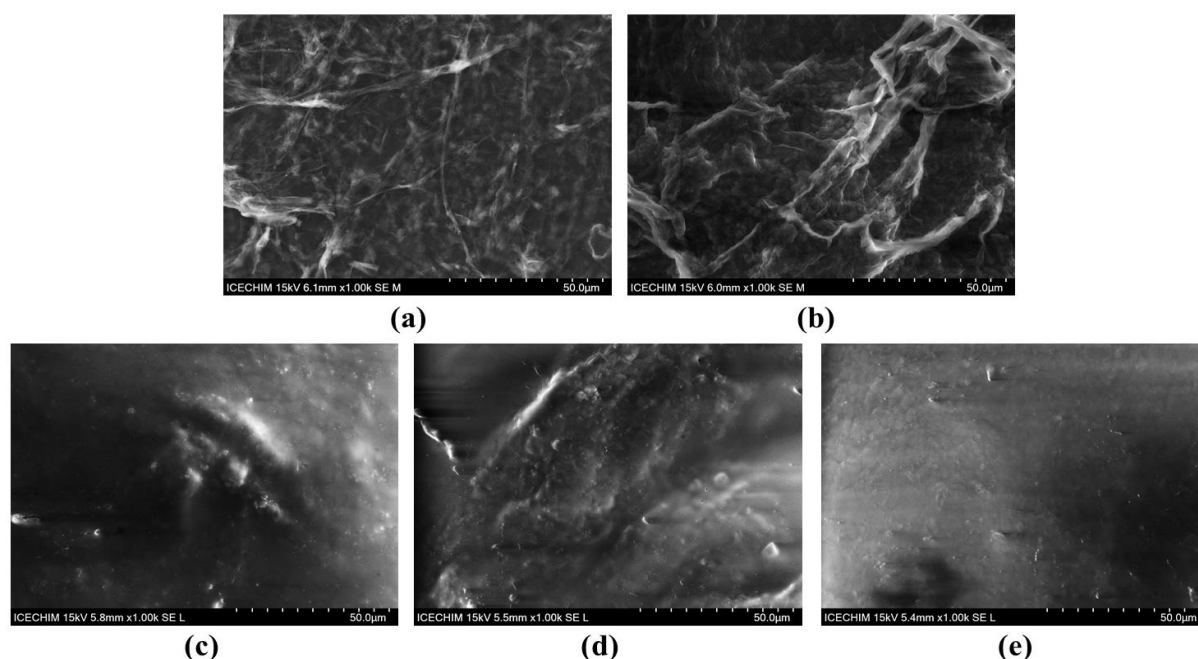


Figure 3. SEM analysis using secondary electrons (SE) detector (1000×) of: (a) VNC, (b) BNC, (c) VNCMu, (d) BNCMu, (e) Mu; VNC – hydrogel of vegetal nanocellulose from brewer's spent grains-based hydrogel; BNC – hydrogel of bacterial nanocellulose from Kombucha fermentation-based hydrogel; VNCMu – VNC mixed with a 3.5% mucin suspension in a ratio of 1:1 (v/v); BNCMu – BNC mixed with a 3.5% mucin suspension in a ratio of 1:1 (v/v); Mu – mucin suspension.

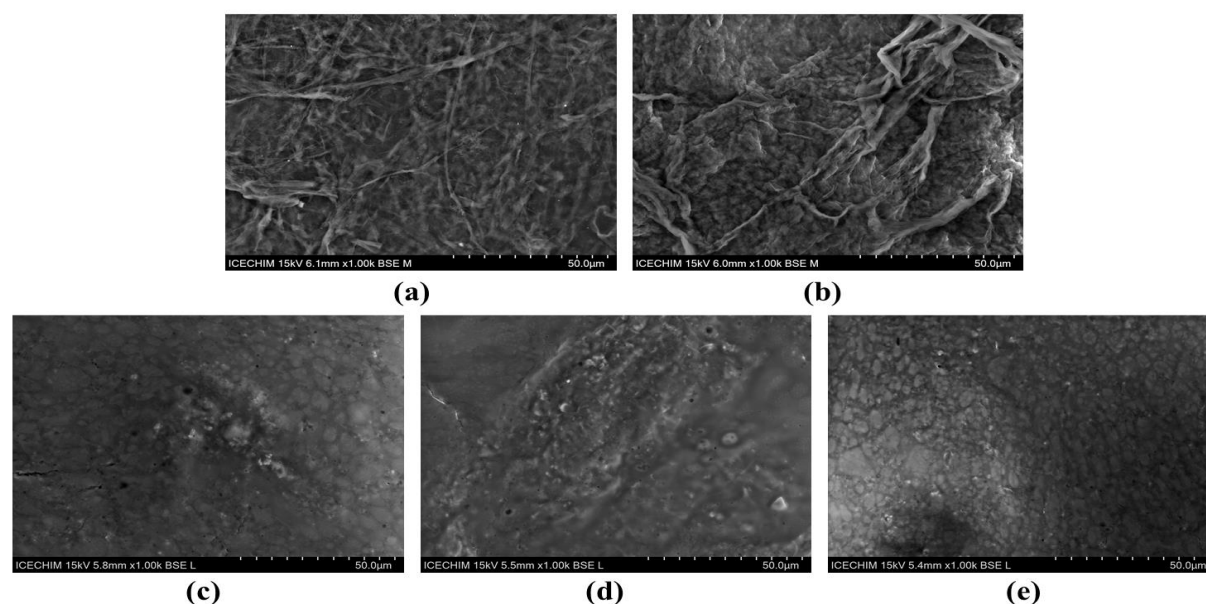


Figure 4. SEM analysis using backscattered electrons (BSE) detector (1000×) of: (a) VNC, (b) BNC, (c) VNCMu, (d) BNCMu, (e) Mu; VNC – hydrogel of vegetal nanocellulose from brewer's spent grains; BNC – hydrogel of bacterial nanocellulose from Kombucha fermentation; VNCMu – VNC mixed with a 3.5% mucin suspension in a ratio of 1:1 (v/v); BNCMu – BNC mixed with a 3.5% mucin suspension in a ratio of 1:1 (v/v); Mu – mucin suspension.

It was previously reported that by alkaline treatment, followed by bleaching and microfluidization, lattice-type cellulose nanofibrils were obtained from brewer's spent grains, with at least 10 microfluidization cycles being necessary in order to produce a uniform fibrillar structure, as

evidenced by SEM analysis [29]. In our case, 10 cycles induced defibrillation, but the structure was not sufficiently uniform. Moreover, in the case of the bacterial cellulose from Kombucha, we previously tested 1, 10, and 20 microfluidization cycles. Defibrillation of the microfibrillar structure of the bacterial cellulose into nanofibrils was obtained after 20 microfluidization cycles based on the XRD analysis. [30]. Therefore, in the present study we used 20 cycles of microfluidization in order to obtain the bacterial as well as the vegetal nanocellulose. At 20 cycles, the vegetal cellulose was defibrillated similarly to the bacterial cellulose as shown in Figure 2.

Following the hydrogel-mucin interaction, a relatively compact structure was obtained for both VNCMu (Figure 3c, 4c) and BNCMu (Figure 3d, 4d), which is similar to the morphological aspect of mucin (Figure 3e, 4e), but with some protuberances. The mucoadhesive properties of vegetal cellulose nanofibers / nanocrystals and the morphological characteristics of the complexes have been previously analyzed not by SEM, but by confocal microscopy [31]. The authors mixed a suspension of Fluorescent Brightener 28-labeled nanocellulose / nanocrystals from bleached softwood kraft pulp with Acridine Orange-labeled pig mucus, followed by rinsing of the hydrogel-mucin system with digestive juice. A significant adhesion of both nanocellulose and nanocrystals to the porcine mucosal layer in simulated gastric and intestinal fluids was observed. Moreover, due to the fibrillar structure of the nanocellulose, cellulose nanofibrils were entangled within the mucus layer, whereas in the case of the cellulose nanocrystals, a more homogeneous structure was obtained, the nanocrystals being spread over the mucus layer.

The wide-angle X-Ray scattering (XRD-WAXS) results of vegetal nanocellulose and bacterial nanocellulose before and after its interaction with mucin are presented in Figure 5. The diffraction spectra were compared with the diffraction patterns of known cellulose allomorphs, available in the PDF5+ PDXL Rigaku database, respectively one-chain triclinic I α (PDF card No. 00-056-1719), two-chain monoclinic I β (PDF card No. 00-060-1502) and amorphous cellulose (PDF card No. 00-060-1501). One-chain I α allomorph prevails in bacterial cellulose and green algae, reason for which it is known as bacterial-algal cellulose, or *Acetobacter-Valonia* cellulose [32–34]. Two-chain I β allomorph prevails in higher plants and it is known as cotton-ramie cellulose. VNC from BSG showed a main diffraction peak at approx. 22.60°, corresponding to cellulose I β , and a predominantly amorphous character attributed to amorphous cellulose, with the crystallinity index (Xc) determined to be 35% (Figure 5a).

The diffractogram of BNC presented in Figure 5b evidenced the crystallographic patterns of cellulose I α with the characteristic peak at 16.76°. The first peak at 14.50° represents the convolution of peak I α at 14.26° and peak I β at 14.83°. Similarly, the main peak at 22.66° is a convolution between peak I α at 21.8° and peak I β at 22.71°. The biosynthesis conditions of present BNC were similar with the ones previously reported [28,35], therefore the spectra are similar in peak position and relative intensities. Under different fermentation conditions the relative peak intensities, correlated with the I α : I β ratio, suffer particular changes [36].

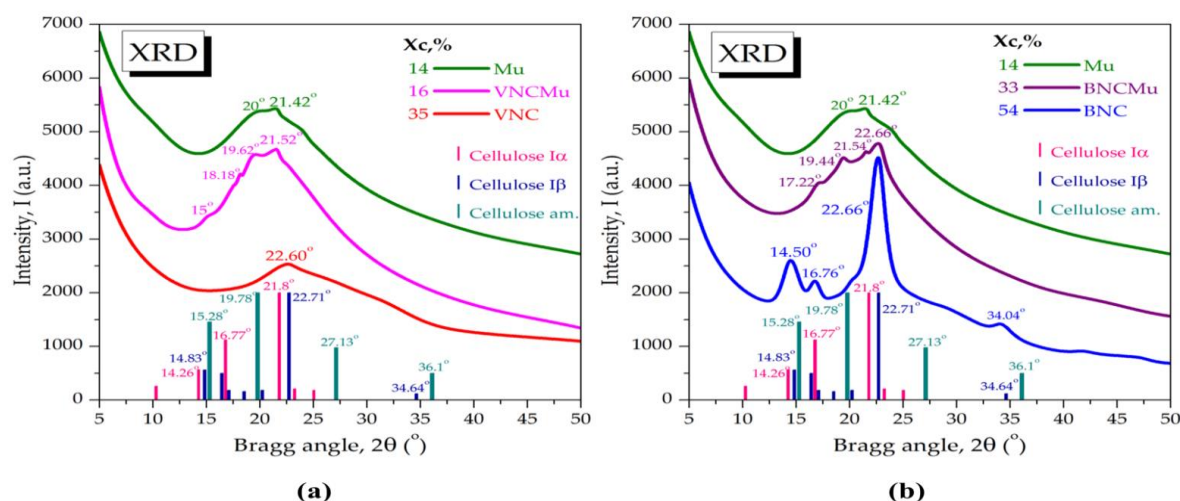


Figure 5. X-Ray diffraction (XRD) analysis and crystallinity index (Xc,%) of: (a) VNC, Mu, VNCMu; (b) BNC, Mu, BNCMu; The vertical bars represent the main diffraction peaks of cellulose I α , I β and

amorphous cellulose in the PDXL database; VNC – hydrogel of vegetal nanocellulose from brewer's spent grains ; BNC – hydrogel of bacterial nanocellulose from Kombucha fermentation; VNCMu – VNC mixed with a 3.5% mucin suspension in a ratio of 1:1 (v/v); BNCMu –BNC mixed with a 3.5% mucin suspension in a ratio of 1:1 (v/v); Mu – mucin suspension.








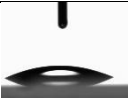







The WAXS diffractogram of mucin showed two main peaks at approx. 20° and 21.42° and a highly amorphous character, with 14% Xc. Individual diffractograms of mucin are apparently scarce since mucin is generally considered completely amorphous [37,38], although in some cases it showed a sharp peak around 27°[39]. The mucin spectrum in Figure 5 is somewhat similar with the one considered completely amorphous, with the main peak at approx. 22° and additional small peaks [37]. In one of our previous studies [40], the same mucin showed a similar diffractogram with the one in Figure 4, but with the two main peaks at approx. 19.50° and 21.52° and two additional small peaks at approx. 6° and 9°, which could be related to the crystallization / lyophilization step. In another study, by small-angle X-ray scattering (XRD-SAXS) it was evidenced that MUC5AC mucin at 1 mg/mL concentration and pH 7 had a gyration radius of 42 ± 4 nm, whereas at the boundary gelation pH of 3.5 the gyration radius decreases to 23 ± 3 nm [32].

The physical interaction between VNC and mucin led to the predominantly amorphous system VNCMu with 16% Xc and with four small diffraction peaks around 2θ angles 15°, 18.18°, 19.62° and 21.52°. The new peaks suggest particular macromolecular interactions with the amorphous cellulose fragments and Iβ chains, which leads to a new distinct structure. In Figure 5b, the crystallinity of BNCMu (33%) is higher than that of VNCMu which indicates a more ordered structure of BNCMu than of VNCMu. The shifted peaks at 17.22° and 21.54° revealed the mucin interaction with the cellulose Ia chains, the shifted peak at 19.44° suggests the interaction with the amorphous cellulose. The IaIβ composite structure at 22.66° appears partially covered, but unshifted.

The VNC hydrogel and BNC hydrogel presented a surface tension of 50.44 ± 0.66 mN/m and 55.29 ± 0.29 mN/m, respectively.. A higher surface tension, as shown for the BNC suspension, correlates with a higher stability of the suspension and also with a higher resistance to flow deformation [41]. A lower surface tension, as for VNC suspension, correlates with an easier separation of the hydrophilic / hydrophobic cellulose fragments. The cellulose concentration, electrostatic charge and fiber length influence the surface tension. A 5% microcrystalline cellulose suspension at pH 4.0, with rod dimensions of 180 ± 30 nm length and 8 ± 3 nm diameter, showed a surface tension of ca. 66.2 ± 0.5 mN/m [41]. VNCMu recorded a significant decrease of 8.37±0.78% in the surface tension compared with VNC. The decrease (12.28 ± 0.97%) in surface tension of BNCMu with respect to BNC was higher (σ=0.006) in comparison with the decrease of VNCMu. Mu showed the lowest surface tension among the samples, i.e., 39.33 ± 0.47 mN/m and induced the decreases mentioned above.

The VNC hydrogel had a contact angle of 52.70 ± 0.56° and 56.90 ± 0.40° on the hydrophilic surface (polar, glass), and on the hydrophobic (non-polar, polystyrene) surface. This suggests an amphiphilic nature of VNC, with a small tendency towards hydrophilicity. The amorphous anisotropic cellulose is known to be more hydrophobic [41]. In the case of VNCMu, the contact angle on the hydrophilic surface decreased by 3.42 ± 0.68% and on the hydrophobic surface increased by 2.18 ± 0.73% compared with VNC. The BNC hydrogel presented a contact angle of 48.27 ± 0.57° and 65.13 ± 0.35° on the hydrophilic surface and on the hydrophobic surface, respectively. This indicates a more hydrophilic character of BNC compared with VNC.. For BNCMu a slightly higher decrease of the contact angle on the polar surface (3.59 ± 1.14%), as well as a significantly higher increase (σ=0.01) on the non-polar surface (4.40 ± 0.41%) were observed compared to the decrease, respectively increase, recorded in the case of VNCMu. The contact angle on both surfaces was determined for the mucin suspension as well. Due to the predominantly hydrophilic nature of mucin [33], the contact angle on the hydrophilic surface was 45.67 ± 0.71° and on the hydrophobic surface the contact angle was significantly higher, i.e., 78.27 ± 0.45° (Table 1).

Table 1. Surface tension and contact angles of nanocellulose-based hydrogels (VNC and BNC) and hydrogel-mucin systems (VNCMu and BNCMu) ± standard error (n=3, α<0.05).

Sample	Surface tension (mN/m)		Contact angle/ hydrophilic surface (°)		Contact angle/ hydrophobic surface (°)	
VNC*	50.44±0.66, <i>d**</i>		52.70±0.56, <i>d</i>		56.90±0.40, <i>a</i>	
VNCMu	46.22±0.39, <i>b</i> (8.37±0.78% decrease)		50.90±0.03, <i>c</i> (3.42±0.68% decrease)		58.14±0.41, <i>b</i> (2.18±0.73% increase, a)	
BNC	55.29±0.29, <i>e</i>		48.27±0.57, <i>b</i>		65.13±0.35, <i>c</i>	
BNCMu	48.50±0.54, <i>c</i> (12.28±0.97% decrease)		46.53±0.55, <i>a</i> (3.59±1.14% decrease)		68.00±0.26, <i>d</i> (4.40±0.41% increase)	
Mu	39.33±0.47, <i>a</i>		45.67±0.71, <i>a</i>		78.27±0.45, <i>e</i>	

*VNC – hydrogel of vegetal nanocellulose from brewer's spent grains; BNC – hydrogel of bacterial nanocellulose from Kombucha fermentation; VNCMu – VNC mixed with a 3.5% mucin suspension with a ratio of 1:1 (v/v); BNCMu – BNC mixed with a 3.5% mucin suspension with a ratio of 1:1 (v/v); Mu – mucin suspension. **Different letters in italics indicate statistically significant differences between samples.

BNC had a significantly higher mucin binding efficiency ($92.85 \pm 2.62\%$ and $82.18 \pm 2.22\%$ at a nanocellulose/mucin ratio (mg/mg) of 12 and 4, respectively) compared to VNC ($74.45 \pm 2.54\%$ and $46.66 \pm 1.47\%$ at a nanocellulose/mucin ratio (mg/mg) of 12 and 4, respectively), as shown in Figure 6. This may be due to the higher hydrophilicity of bacterial nanocellulose, which suggests a higher availability of hydroxyl groups. This allows a stronger interaction between the free -OH groups of the bacterial nanocellulose and the mucin glycoproteic structure. The higher availability of free -OH groups correlates with $I\alpha$ cellulose allomorph found in BNC and with the cellulose fragments that compose the amorphous cellulose. The stronger $I\beta$ allomorph, predominant in VNC has a higher number of hydroxyl groups involved in hydrogen bridges between the two chains [28]. Additionally, the fibrillar structure of BNC is more developed, with longer chains compared to VNC [28,42]. The longer nanofibrils entangle with the branched structure of mucin and therefore increase the mucoadhesion.

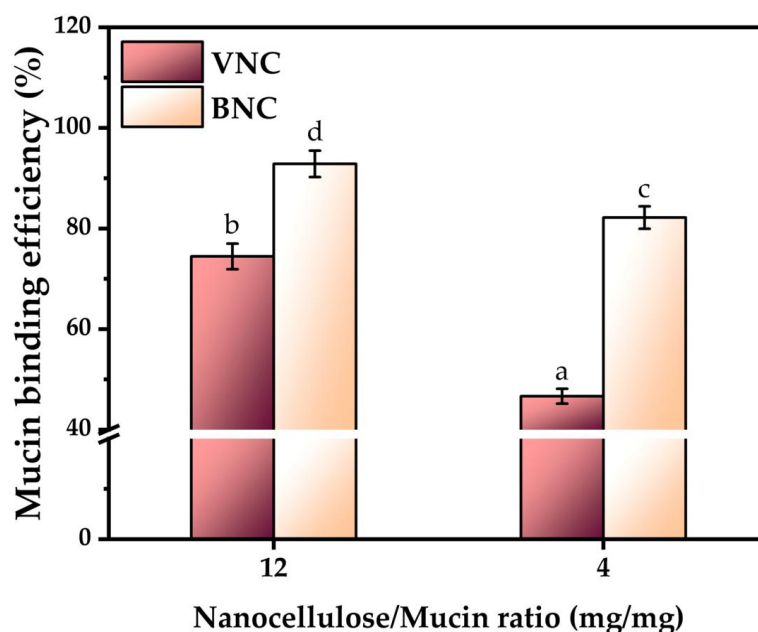


Figure 6. Mucin binding efficiency (\pm standard deviation, $n=3$, $\alpha<0.05$; different letters indicate statistically significant differences between samples); VNC – hydrogel of vegetal nanocellulose from brewer's spent grains; BNC – hydrogel of bacterial nanocellulose from Kombucha fermentation.

The viscoelastic behavior of the VNC and BNC suspensions observed by the rheological experiments performed in frequency sweep, flow sweep and axial mode are depicted in Figure 7. The oscillatory or frequency sweep mode presented in Figure 6a and b allows the evaluation of storage modulus G' , loss modulus G'' , complex viscosity η^* , dynamic viscosity η' and phase angle δ in the chosen range of 0.1-100 rad/s angular frequencies ω . The storage modulus describes the elastic contribution, meaning the solid-like behavior of the suspension, whereas the loss modulus describes the viscous contribution, meaning the liquid-like behavior. The complex modulus $|G^*|$ describes the overall resistance to deformation of the suspensions, including the elastic, recoverable, deformation and the viscous, non-recoverable, deformation, and if divided by the angular frequency ω , it gives the complex viscosity η^* . Both VNC and BNC suspensions showed in Figure 7a and b a higher storage modulus than loss modulus, this fact being generally considered a gel property [43]. BNC showed higher storage and loss modulus values than VNC, respectively a mean $G'=28.26$ Pa and $G''=3.92$ Pa at 4 rad/s for BNC compared with a mean $G'=0.88$ Pa and $G''=0.13$ Pa at 4 rad/s for VNC. In another study, a 1% microcrystalline-derived nanocellulose suspension of 211 ± 114 nm fibrils showed a storage modulus of approx. 40 Pa and a loss modulus of approx. 9 Pa [44]. Another difference between VNC and BNC consists in the storage modulus exponential, which increased for VNC at angular frequencies higher than 10 rad/s, up to 18.67 Pa at 100 rad/s, whereas the BNC storage modulus slowly increases up to 59.83 Pa at $\omega=100$ rad/s. The loss modulus G'' showed a sinusoidal increasing trend for both VNC and BNC, with a maximum value of $G''=0.26$ Pa at 25.12 rad/s for VNC, respectively $G''=5.75$ Pa at 63.10 rad/s for BNC. The initial complex viscosity of BNC ($\eta^*=213.66$ Pa·s) is approx. 33 times higher than that of VNC ($\eta^*=6.48$ Pa·s). The complex viscosity of BNC suspension constantly decreases with the increasing of the angular frequency ω . This behavior evidences a shear thinning (pseudoplastic) behavior, which typically suggests the orientation and disentanglement of the nanofibers [44]. The VNC suspension is pseudoplastic up to 25.12 rad/s and becomes shear thickening (dilatant) at higher ω , probably because of amorphous cellulose disordering and fragments intercalation. The oscillatory hysteresis loop is not significant, showing only a slight thixotropic behavior for VNC. This is evidenced as a small decrease of the complex viscosity on the reverse ramp, a small decrease of the storage modulus, and a small increase of the loss modulus and of phase angle δ . High values of phase angle δ correlate with a viscous, liquid behavior, whereas low values of δ suggest an elastic, solid-like behavior [40].

At higher shear rates in flow sweep mode depicted in Figure 7c and d, both nanocellulose suspensions show a complex behavior with strong hysteresis. The steady state viscosity η decreases in the shear rate $\dot{\gamma}^*$ range of 1-4 1/s for VNC from 3.03 Pa·s to 0.08 Pa·s, after which increases to a maximum of 0.27 Pa·s at $\dot{\gamma}^*=10$ 1/s and decreases again to 0.01 Pa·s at $\dot{\gamma}^*=100$ 1/s. A critical shear rate around $\dot{\gamma}^*=5$ 1/s was previously observed for other nanocellulose suspensions [44]. For BNC, η constantly decreases from 37.10 Pa·s at $\dot{\gamma}^*=0.1$ 1/s to 0.01 Pa·s at $\dot{\gamma}^*=100$ 1/s. The viscosity of vegetal nanocellulose suspensions is known to be very high due to fibril length and entanglement. A 0.7% suspension of fibrils with a medium length of 820 ± 570 nm showed a viscosity of approx. 4 Pa·s, whereas a 1% suspension of 211 ± 114 nm fibrils showed a viscosity of approx. 2 mPa·s at $\dot{\gamma}^*=1$ 1/s [44]. The hysteresis loop is significant for both nanosuspensions, showing a stronger thixotropy for VNC than BNC. The thixotropy of nanocellulose water suspensions depends on the structural hierarchy and concentration of the nanoparticles, some possible hierarchies being individual nanoparticles, mesophase liquid crystalline domains, chiral nematic and nematic structures [43].

The thixotropic behavior is more pronounced at higher concentrations [43] and for the macromolecular structures with higher molar weights, whereas the rheopectic or anti-thixotropic behavior generally appears in amphiphilic systems due to repeated disequilibrium states between hydrophilic and hydrophobic components induced by shearing. The thixotropy is proportional with the hysteresis loop [43], VNC suspension being more thixotropic than BNC as can be seen in Figure 7c and d. The Carreau-Yasuda rheological model fits best the viscosity variation for both VNC and BNC suspensions, whereas the Herschel-Bulkley fitting model describes a Bingham fluid with yield stress above which the hydrogel starts to flow, the yield stress being 8 times higher for BNC (0.50 Pa) than for VNC (0.06 Pa). The yield stress can be considered as a stability parameter and as an intrinsic resistance to flow deformation, and it can be correlated with the surface tension, higher for BNC than for VNC, as previously determined.

The adhesion force determined in Figure 7e and f as the axial force that opposes the detachment with 10 $\mu\text{m/s}$ lifting speed of the cylindrical geometry from the nanosuspensions shows a higher value of 0.154 N for BNC compared with 0.128 N for VNC. The adhesion time is higher for VNC, with 46 s adhesion time at maximum axial force and 524 s total adhesion time, in comparison with 29 s adhesion time at maximum axial force and 467 s total adhesion time for BNC, which suggests more contact points with the quartz and geometry surfaces for VNC than for BNC. The speed of detachment evaluated as the exponential parameter c is higher for VNC than for BNC, the axial experiment conclusively suggesting multiple short nanofibrils in VNC in comparison with fewer but longer nanofibrils in BNC, considering the same cellulose concentration.

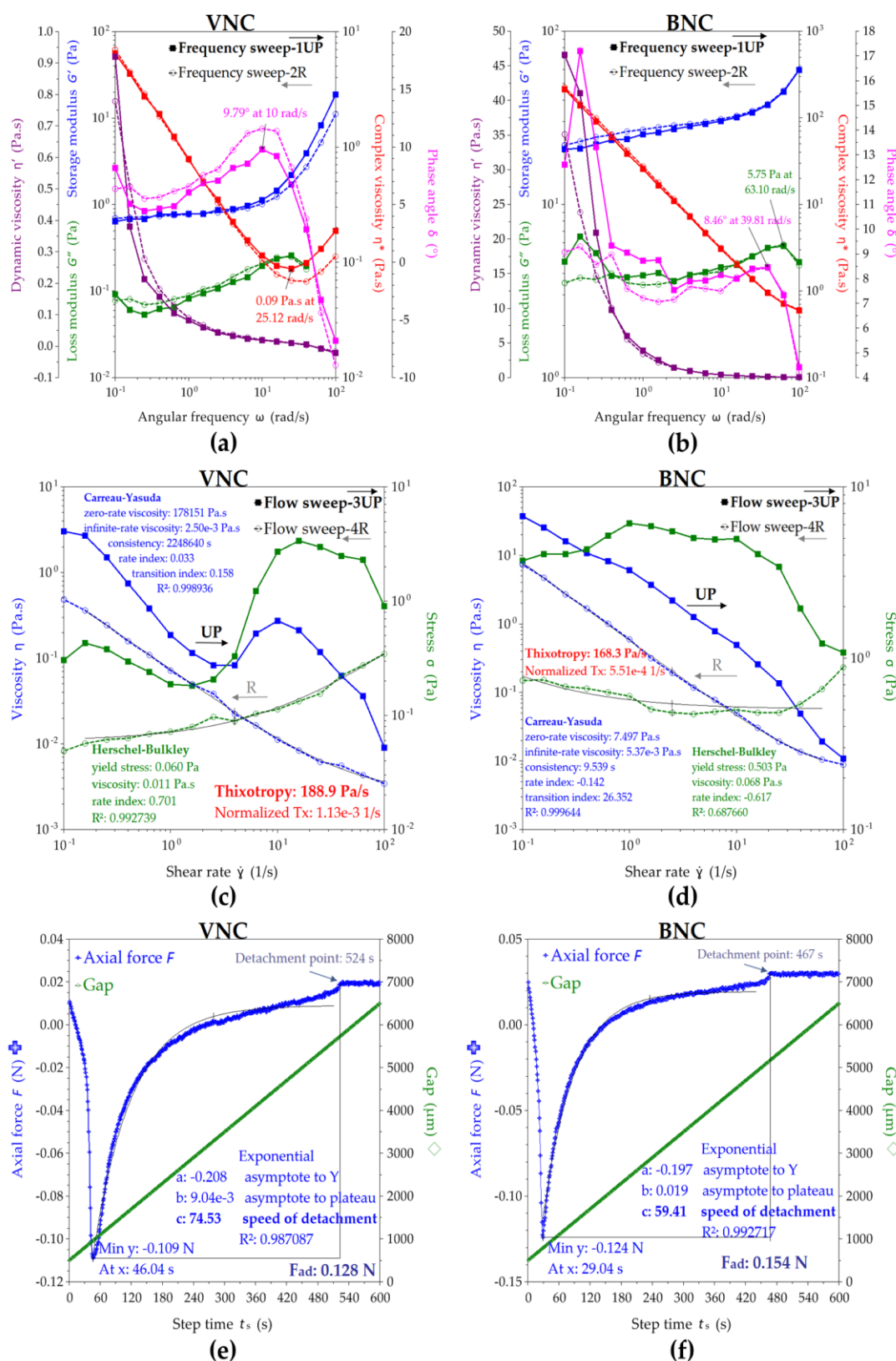


Figure 7. Rheological behavior of VNC and BNC hydrogels: (a) Frequency sweep of VNC; (b) Frequency sweep of BNC; (c) Flow sweep of VNC; (d) Flow sweep of BNC; (e) Axial mode of VNC; (f) Axial mode of BNC; VNC – hydrogel of vegetal nanocellulose from brewer's spent grains; BNC – hydrogel of bacterial nanocellulose from Kombucha fermentation.

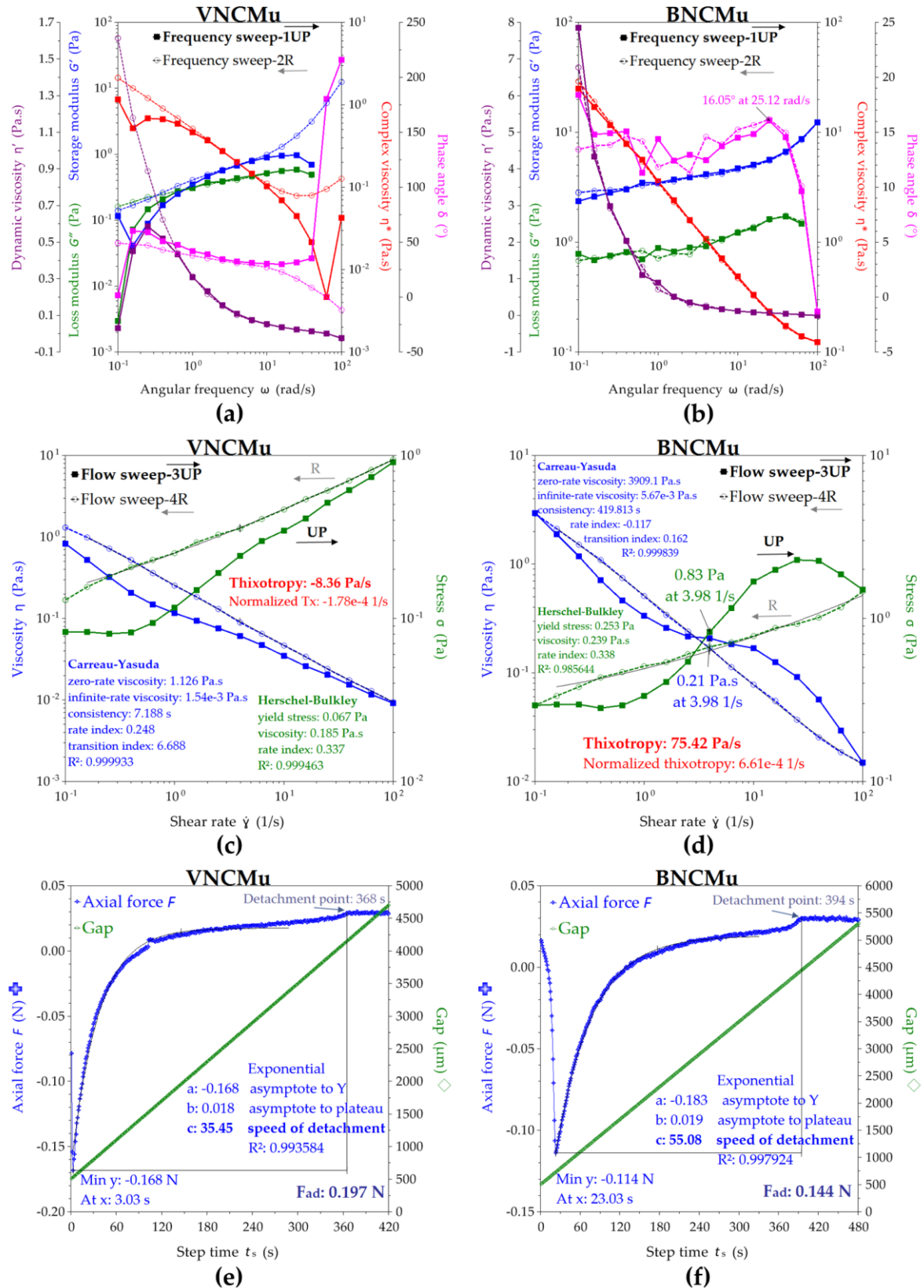


Figure 8. Rheological behavior of VNCMu and BNCMu: (a) Frequency sweep of VNCMu; (b) Frequency sweep of BNCMu; (c) Flow sweep of VNCMu; (d) Flow sweep of BNCMu; (e) Axial mode of VNCMu; (f) Axial mode of BNCMu; VNCMu – hydrogel of vegetal nanocellulose from brewer's spent grains mixed with a mucin suspension in a ratio of 1:1 (v/v); BNCMu – hydrogel of bacterial nanocellulose from Kombucha fermentation mixed with a mucin suspension in a ratio of 1:1 (v/v).

These results correlate with the XRD, surface tension and contact angle results. Shorter and multiple VNC fibrils correlate with an amorphous character, lower surface tension, amphiphilic character due to exposed hydrophobic glucose rings and methyl-rich chain ends [45,46] and multiple surface adhesion points, both hydrophilic -OH functional groups and hydrophobic glucose rings. Longer and fewer BNC nanofibrils correlate with a higher crystallinity, higher surface tension due to chain length, higher hydrophilicity, more cohesive points through glucose ring-ring Van der Waals interactions combined with intra- and intermolecular hydrogen bonds, and respectively fewer surface adhesion points inducing a lower adhesion time.

The rheology of mucin mixtures with VNC and BNC nanosuspensions is depicted in Figure 8. Mucin is a high molecular weight branched glycoprotein and, rich in different functional groups able to establish many hydrogen bonds with all types of compounds and surfaces. The mucin rheology depends on source, pH, concentration, temperature, time and shear rate [40,47,48]. At pH lower than 4, mucin has a gel or solid-like behavior with $G' > G''$, and at higher or neutral pH mucin has a viscous liquid-like behavior [40,48]. In oscillatory shearing mode presented in Figure 8a and b, VNCMu showed a viscoelastic behavior with G' close to G'' up to $\omega=2.51$ rad/s, angular frequency from which the elastic behavior becomes dominant. BNCMu is more elastic than VNCMu, with G' higher than G'' , due to the BNC influence having longer cellulose nanofibrils.

In flow sweep experiments presented in Figure 8c, the VNCMu suspension shows a reopectic behavior, with viscosity increasing on the reverse curve. In Fig. 8d, the BNCMu suspension showed a complex thixotropic behavior, with a critical shear rate around 4 1/s. Both suspensions with mucin present a yield stress determined by the Herschel-Bulkley model and it is higher for BNCMu than for VNCMu.

The axial experiments presented in Figure 8e,f evidenced the adhesion force of VNCMu ($F_{ad}=0.197$ N) to be higher than that of BNCMu and the initial VNC suspension, which suggests a stronger interaction between BNC and Mu than between VNC and Mu. The adhesion times decrease in the cellulose-mucin system, suggesting that a part of the initial adhesion energy of VNC and BNC suspensions induced by the multitude of hydroxyl groups was transformed in cohesion energy with the glycoproteic functional groups of mucin.

2.2. The Cytocompatible Behaviour of Nanocellulose-Based Hydrogels

A high degree of cytocompatibility of BNC was observed at all tested concentrations in comparison with the negative cytotoxicity control (C-, untreated cells). Significant increases in the number of metabolically active viable cells were recorded at the lowest concentrations of BNC tested, i.e., $104.48 \pm 0.31\%$ of C- at 0.0125% (w/v) BNC and $107.60 \pm 0.98\%$ of C- at 0.025% (w/v) BNC (Figure 8a). At concentrations between 0.0125-0.05% (w/v), VNC exhibited a high degree of cytocompatibility, with a significant increase in the cell viability at the lowest concentration tested ($104.67 \pm 1.02\%$ of C- at 0.0125% VNC). Higher concentrations of VNC led to a statistically significant reduction in the cell viability, i.e., $94.38 \pm 0.61\%$ of C- at 0.1% (w/v) VNC and $89.36 \pm 0.74\%$ of C- at 0.2% VNC (Figure 9a).

Thus, at the lowest concentration tested, i.e., 0.0125% (w/v), there are no significant differences between the two hydrogels, both being equally efficient with respect to the cytocompatible behavior. By increasing the concentration, only the hydrogel of bacterial nanocellulose led to a further significant increase in the cell viability, showing its high potential to support tissue regeneration. The results from Figure 8a obtained after performing the CCK-8 assay can be correlated with the fluorescence microscopy images shown in Figure 9b-m acquired after performing the LIVE/DEAD assay.

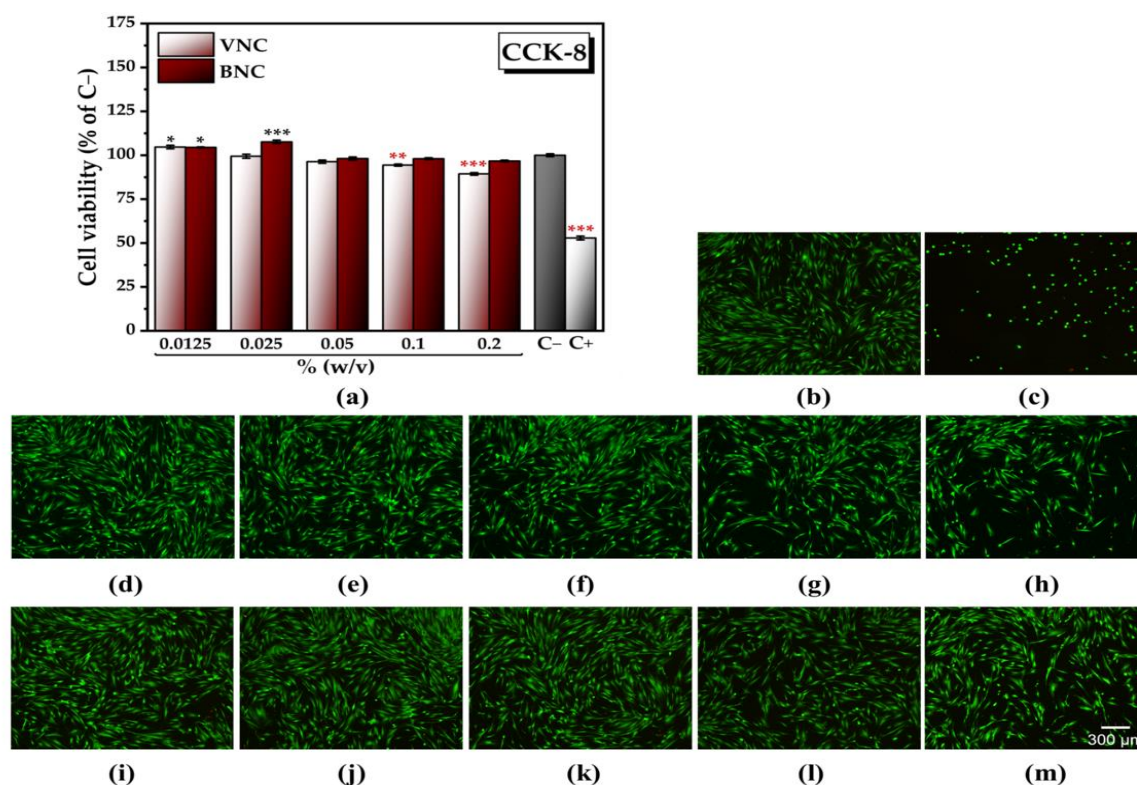


Figure 9. Cytocompatibility of VNC and BNC hydrogels: (a) Cell Counting Kit-8 (CCK-8) assay (\pm error bars, $n=3$, $\alpha<0.05$; *— σ between 0.05 and 0.01, **— σ between 0.01 and 0.001, and ***— $\sigma < 0.001$; black stars indicate statistically significant values that exceed C-; red stars indicate statistically significant values that are below C-; C- (untreated cells, negative cytotoxicity control), C+ (cells treated with 7.5% dimethyl sulfoxide (DMSO), positive cytotoxicity control), VNC – hydrogel of vegetal nanocellulose from brewer's spent grains; BNC – hydrogel of bacterial nanocellulose from Kombucha fermentation; (b-h) LIVE/DEAD assay (live cells – green fluorescence, dead cells – red fluorescence): (b) C-; (c) C+; (d) Cells treated with 0.0125% (w/v) VNC; (e) Cells treated with 0.025% (w/v) VNC; (f) Cells treated with 0.05% (w/v) VNC; (g) Cells treated with 0.1% (w/v) VNC; (h) Cells treated with 0.2% (w/v) VNC; (i) Cells treated with 0.0125% (w/v) BNC; (j) Cells treated with 0.025% (w/v) BNC; (k) Cells treated with 0.05% (w/v) BNC; (l) Cells treated with 0.1% (w/v) BNC; (m) Cells treated with 0.2% (w/v) BNC.

Fluorescence microscopy images acquired after labelling of the actin filaments and the nuclei showed no changes in cell morphology following treatment with 0.025% (w/v) VNC and BNC (Figure 10b,c), compared with the negative cytotoxicity control (Figure 10a). The cytoskeleton is well organized in a fibrillar structure with numerous actin filaments, with the cells maintaining their characteristic phenotype.

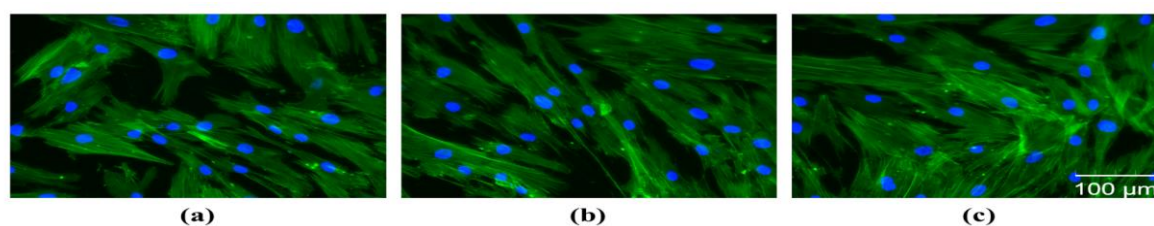


Figure 10. Cell morphology following the treatment with VNC and BNC hydrogels (Alexa Fluor 488-coupled phalloidin labelling of the actin filaments – green fluorescence, and DAPI labelling of the nuclei – blue fluorescence): (a) Untreated cells, negative control; (b) Cells treated with 0.025% (w/v)

VNC; (c) Cells treated with 0.025% BNC; VNC – hydrogel of vegetal nanocellulose from brewer's spent grains; BNC – hydrogel of bacterial nanocellulose from Kombucha fermentation.

It was previously demonstrated that the length of the nanocellulose fibers represents an important factor with respect to the cytocompatible behaviour [49]. In the Hepa 1-6 and KUP5 liver cells, the long nanocellulose fibers with the chain length of about 6000-7000 nm presented a high degree of cytocompatibility at concentrations between 25-200 $\mu\text{g/mL}$. There was only a slight decrease in the viability of the KUP5 cells at the highest concentration tested. Short nanocellulose fibers with the chain length of about 100-600 nm induced significant decreases in the viability of KUP5 cells, especially at the highest concentrations tested by the authors. Hepa cells 1-6 were affected only by the short fibers of about 175 nm, pointing also to a cytotoxic effect which is correlated with the cell type [49]. Moreover, long nanocellulose fibers organized in a mesh-like structure can support the adhesion, growth and differentiation of the cells, leading to an increase in the number of metabolically active viable cells, promoting tissue regeneration [50].

3. Conclusions

Two types of hydrogels based on vegetal nanocellulose from brewer's spent grains (VNC) and, respectively, bacterial nanocellulose from Kombucha fermentation (BNC) were obtained. Morphological analyses showed a denser fibrillar structure with longer cellulose nanofibers in the case of BNC, compared to VNC. BNC showed higher crystallinity and hydrophilicity than VNC. The mucin binding efficiency of the BNC hydrogel was significantly higher ($92.85 \pm 2.62\%$ and $82.18 \pm 2.22\%$ at a nanocellulose/mucin ratio (mg/mg) of 12 and 4, respectively) in comparison with the VNC hydrogel ($74.45 \pm 2.54\%$ and $46.66 \pm 1.47\%$ at a nanocellulose/mucin ratio (mg/mg) of 12 and 4, respectively). The interaction between BNC and mucin was stronger compared to the interaction between VNC and mucin based on rheological analysis.

The BNC hydrogel presented a high degree of cytocompatibility for all the concentrations tested. At 0.025% (w/v) BNC hydrogel, the highest increase in the number of metabolically active viable cells, i.e., $107.60 \pm 0.98\%$ of cytotoxicity negative control was recorded. This suggests that the BNC hydrogel represents an excellent and better than VNC candidate for various biomedical nanoformulations. Kombucha SCOBY should be considered as a cost-effective source of bacterial cellulose, but new, more environment-friendly purification processes should be developed.

4. Materials and Methods

4.1. Materials

Brewer's spent grains were recovered from the Ursus brewery (Brasov, Romania) after the beer production process. The Symbiotic Culture of Bacteria and Yeasts (SCOBY) pellicles were obtained from a local Kombucha culture [28].

Sodium hydroxide pellets and sodium hypochlorite solution 15% w/v (Scharlau, Barcelona, Spain) were used in order to purify the vegetal and bacterial cellulose.

The mucin binding efficiency was investigated using the following reagents: fuchsin basic for microscopy, hydrochloric acid 1N (Scharlau, Barcelona, Spain), glacial acetic acid, potassium metabisulfite, activated charcoal (Chimreactiv, Bucharest, Romania), mucin from porcine stomach type II (Sigma-Aldrich, St. Louis, MO, USA), periodic acid (VWR International, Pennsylvania, USA).

The investigation of cell viability was performed on human gingival fibroblasts (HGF-1, ATCC CRL-2014) using Cell Counting Kit-8 (Bimake, Houston, TX, USA) and Viability/Cytotoxicity Assay Kit (Biotium, Fremont, CA, USA). The cell morphology was highlighted using Phalloidin-iFluor 488 Reagent (Abcam, Cambridge, United Kingdom) and 4',6-diamidino-2-phenylindole, dilactate (DAPI) (Sigma-Aldrich, St. Louis, MO, USA). In order to investigate the cytocompatibility, different buffers or culture media were prepared based on: Dulbecco's Modified Eagle's Medium (DMEM)-low glucose, D-(+)-Glucose, sodium bicarbonate, trypsin from porcine pancreas, dimethyl sulfoxide 99.5%, antibiotic antimycotic solution 100 \times stabilized, trypsin from porcine pancreas (Sigma-Aldrich,

St. Louis, MO, USA), di-sodium hydrogen phosphate dihydrate, sodium dihydrogen phosphate monohydrate, potassium chloride, sodium chloride, paraformaldehyde, Triton X-100, sodium n-dodecyl sulfate 99% (Scharlau, Barcelona, Spain), albumin bovine fraction V, pH 7.0 (Janssen Chimica, Beerse, Belgium), fetal bovine serum (FBS) USDA APPD. ORIGIN (Thermo Fisher Scientific, Waltham, MA, USA).

4.2. Production of Bacterial Cellulose

Bacterial cellulose: the synthesis of bacterial cellulose was induced according to [36]. A tea infusion of 10 g/L black tea in sterile double-distilled water was prepared, then filtered through sterile gauze. The sweetened tea infusion was obtained by adding 80 g/L sugar. The fermentation process was started by adding 10% SCOBY from a previous Kombucha fermented beverage. The jars were left at room temperature for 14 days.

4.3. Production of Bacterial and Vegetal Cellulose Nanofibers

Due to the recalcitrant vegetable biomass, a first stage of purification was necessary in the case of BSG. BSG was ground with a Retsch Type S 100 centrifugal mill (Haan, Germany). In order to remove the extractables, BSG was mixed with a solution of 2:1 toluene:ethanol (v/v) in a ratio of 1:20 (w/v) and kept for 6 h at 90°C, 250 rpm, in a laboratory reflux installation. Subsequently, the resulting precipitate was centrifuged in an Universal 320R Centrifuge (Hettich, Tuttlingen, Germany) at 12°C, 7350 ×g for 30 min and freeze-dried for 24 h using a ScanVac CoolSafe 55-4 freeze-dryer (LaboGene, Bjarkesvej, Denmark), at a working temperature -55°C.

In order to obtain the vegetal and bacterial nanocellulose, the bacterial cellulose and pretreated-BSG underwent a chemical purification process and a mechanical microfluidization process. Kombucha membranes were rinsed with double-distilled water and gently chopped before starting the treatments.

The purification process was performed according to [51]. Kombucha membranes and pretreated-BSG were mixed with a solution of 1M NaOH at a ratio of 2.5 (w/v) and kept at a temperature of 90°C for 1 h, under stirring (250 rpm). The alkaline solution was removed, and the samples were thoroughly washed with double-distilled water. The alkaline treatment was repeated keeping the same parameters (90°C, 1h, 250 rpm), as well as the washing process. The washed samples were mixed with a solution of 1.5 % NaClO and kept for 2 h at room temperature, under stirring (250 rpm), then washed very well with double-distilled water. For a more effective purification, 4 ultrasound cycles of 6h each were applied on the washed samples in water with an ultrasound bath Elmasonic P30H (Singen, Germany) using the following parameters: 60°C, 37 pulses/min, 100 W power.

The purified samples were subjected to a milling process using a blender. Suspensions of 6% wet substance (0.06% dry matter) were prepared with double-distilled water and underwent a mechanical process of 20 passes using a microfluidizer (Microfluidics, Westwood, MA, USA).

4.4. Preparation of VNC- / BNC Hydrogels, and Hydrogel-Mucin Systems

Nanocellulose from brewer's spent grains, as well as from Kombucha fermentation synthesized in Section 4.3. were concentrated in a Rotavapor R-300 system (BUCHI Corporation, New Castle, DE, USA) up to a concentration of 0.4% dry matter using the following parameters: 60°C evaporation temperature with a chiller stage at 20°C, 40 rpm, 100 bar pressure, which resulted in VNC and BNC samples.

In order to assess the physicochemical properties of the hydrogel-mucin system, a suspension of 3.5% mucin was prepared in double-distilled water. After the complete homogenization of the suspension according to [40], it was mixed with VNC- and BNC hydrogels at a ratio of 1:1 (v/v), which resulted in VNCMu and BNCMu samples.

For the analyses where it is mentioned that the samples were freeze-dried, the same parameters mentioned in Section 4.3. were used for the freeze-drying process of the VNC, BNC, VNC-Mu, BNC-Mu and Mu samples.

4.4. Physico-Chemical Characterization of the VNC / BNC Hydrogels and Investigation of the Hydrogel-Mucin Interaction

4.4.1. Transmission Electron Microscopy (TEM) Analysis

A small amount of sample (10 μ L) was added on a carbon type-B, 200 mesh copper grid (Ted Pella, Redding, CA, USA). TEM images were acquired with a TECNAI F20 G2 TWIN Cryo-TEM (FEI) transmission electron microscope (Houston, TX, USA) applying an accelerating voltage of 200 kV.

4.4.2. Scanning Electron Microscopy (SEM) Analysis

SEM micrographs of freeze-dried samples were acquired with a TM4000Plus II tabletop electron microscope (Hitachi, Tokyo, Japan) using the following parameters: 15 kV electron acceleration voltage, secondary electrons (SE) / backscattered electrons (BSE) detector, low-charge (L) vacuum mode, 1000 \times magnification.

4.4.3. X-ray Diffraction (XRD) Analysis

The XRD were performed on freeze-dried samples with a Rigaku– SmartLab diffractometer (Rigaku Corporation, Tokyo, Japan) using the following parameters: 40 kV operation voltage, 200 mA emission current, incident $\text{CuK}\alpha_1$ radiation ($\lambda = 1.54059 \text{ \AA}$). A range of 2θ angles 5– 50° with a step of 0.02° and a scan speed of 4°/ min was used in order to obtain the diffractograms. The diffractograms were processed and analyzed in the PDXL software version 2.7.2.0 for the peak identification and calculation of the crystallinity degree (X_c , %) which is the ratio between the area of the crystalline peaks and the area of all peaks.

4.4.4. Interfacial Tension and Contact Angle Assessment

An OCA50 optical tensiometer (DataPhysics Instruments GmbH, Filderstadt, Germany) was used in order to measure the surface tension (mN/m) and the contact angle (°). The measurements were performed in triplicate for each sample using the SCA20 software version 5.0.41.

4.4.5. Investigation of Mucin Binding Efficiency by Periodic ACID SCHIFF (PAS) Assay

The VNC- and BNC hydrogels (0.4% dry matter) were mixed with a suspension of 0.1% mucin prepared in double distilled water (w/v) at a 3:1 and 1:1 (v/v) ratio, then incubated at 37°C (Static Cooled incubator MIR-154 PHCbi, MO, USA) under shaking (Trayster IKA, Staufenim Breisgau, Germany) for 1 h. The samples were centrifuged for 1 h at room temperature, 20,000 \times g. Free mucin in the supernatant was quantified by the PAS reaction [52,53]. The mucin binding efficiency (%) was calculated by subtracting the free mucin concentration from the initial mucin concentration.

4.4.6. Rheological Analysis

Rheological experiments of VNC and BNC suspensions, together with its suspensions with mucin, were performed using a HR20 Discovery Hybrid rotational rheometer from TA Instruments (New Castle, DE, USA) in three different shearing modes with hysteresis (up and reverse rate variation) at 25°C and 500 μ m gap. A sample amount of approx. 0.7 mL, able to fill the 500 μ m gap between the 40 mm geometry and quartz surface, was subjected to a series of UP and reverse (R) oscillation mode in the angular frequency range of ω 0.1-100 rad/s, followed by UP and R linear flow sweep in the shear rate range of 0.1-100 1/s, and ending with the axial mode of geometry rising with constant speed of 10 μ m/s for a duration of 10 min to determine the adhesion force and adhesion time.

4.5. Cytocompatibility Analysis of VNC and BNC

4.5.1. Cell Counting Kit-8 (CCK-8) and LIVE/DEAD Assays

For the investigation of cytocompatibility of nanocellulose-based hydrogels, DMEM was supplemented with 10% FBS. HGF-1 cells were seeded in 48-well plates using a cell density of 1×10^4 cells/cm² and kept at 37°C under 5% CO₂ atmosphere. At 24 h post-seeding, the cells were treated with different concentrations of VNC and BNC hydrogels, i.e., 0.0125, 0.025, 0.05, 0.1, 0.2% dry matter (w/v). Cell viability was determined 24 h post-treatment by combining the CCK-8 and LIVE/DEAD assays according to [30]. In the case of CCK-8 assay, after the incubation time, the liquid was transferred in a 96-well plate and the absorbance was recorded at 450 nm using a microplate reader (CLARIOstar BMG Labtech, Ortenberg, Germany). After performing the LIVE/DEAD assay, HGF-1 cells were visualized using a cell imaging system (Celena® X High Content Imaging System (Logos Biosystems, Gyeonggi-do, South Korea). The image acquisition was performed using Celena® X Explorer software version 1.0.5 (4× objective), and the image analysis was carried out using Celena® X Cell Analyzer version 1.5.2.

4.5.2. Investigation of Cell Morphology

The morphological features of the cells 24 h post-treatment (as in Section 4.5.1.) were highlighted by fluorescent labeling of cytoskeletal actin with Alexa Fluor 488-coupled phalloidin (green) and nuclei with DAPI (blue) according to [30]. The HGF-1 cells were examined using Celena® X High Content Imaging System (Logos Biosystem, Gyeonggi-do). The image acquisition and processing (overlapping fluorescent images of cytoskeletal actin and nuclei) was carried-out using Celena® X Explorer software, 1.0.5 (20× objective). The image analysis was made using Celena® X Cell Analyzer, version 1.5.2.

4.6. Statistical Analysis

Statistical analysis (One-Way ANOVA, Independent Sample T-test) was performed using IBM SPSS 26 software version 26.0.0.0 (IBM Corp., Armonk, NY, USA)

Author Contributions: Conceptualization, D.C.-A. and F.O.; methodology, I.P.-T., F.O., and A.C.; validation, D.C.-A., F.O., and A.C.; formal analysis, I.P.-T., N.T. and S.-O.D.; investigation, I.P.-T., N.T., S.-O.D., B.T., M.G.; resources, F.O. and D.C.-A.; data curation, I.P.-T., N.T., S.-O.D.; writing—original draft preparation, I.P.-T., N.T., and S.-O.D.; writing—review and editing, F.O. and D.C.-A.; visualization, D.C.-A. and A.C.; supervision, F.O., D.C.-A. and A.C.; project administration, F.O. and D.C.-A.; funding acquisition, F.O. and D.C.-A. All authors have read and agreed to the published version of the manuscript.

Funding: This research was funded by project PN 23.06.02.01 InteGral, Nucleu Programme, funded by Ministry of Research, Innovation and Digitalization and project POC-A1-A1.2.3-G-2015-P_40_352-SECVENT, Sequential processes to close bioeconomy side stream and innovative bioproducts resulted from these, contract 81/2016, SMIS 105684, funded by Cohesion Funds of the European Union, subsidiary project 1392/2022 NutriCel.

Institutional Review Board Statement: Not applicable

Informed Consent Statement: Not applicable

Data Availability Statement: All data are presented within the article

Acknowledgments: We thank dr. Valentina Mitran for guidance into the cell culture work and to dr. Ionut Moraru for supply of the SCOBY/Kombucha pellicles. The XRD diffractometer and the cryo-TEM equipment were purchased with the support of the POS-CCE “Agri-Flux” project, nr. 645/18.03.2014, SMIS-CSNR 48695. The scanning electron microscope was acquired in the frame of the project 15PFE Next-Bexcel.

Conflicts of Interest: The authors declare no conflicts of interest.

References

1. Scrivener, C.A.; Schantz, C.W. Penicillin: New Methods for its Use in Dentistry. *The Journal of the American Dental Association* **1947**, *35*, 644-647. <https://doi.org/>.

2. Smart, J.D. The basics and underlying mechanisms of mucoadhesion. *Adv. Drug Deliv. Rev.* **2005**, *57*, 1556-1568. <https://doi.org/10.1016/j.addr.2005.07.001>.
3. Grondin, J.A.; Kwon, Y.H.; Far, P.M.; Haq, S.; Khan, W.I. Mucins in Intestinal Mucosal Defense and Inflammation: Learning From Clinical and Experimental Studies. *Frontiers in Immunology* **2020**, *11*.
4. Bird, D.; Ravindra, N.M. Transdermal drug delivery and patches—An overview. *Medical Devices & Sensors* **2020**, *3*, e10069. <https://doi.org/>.
5. Rath, R.; Tevatia, S.; Rath, A.; Behl, A.; Modgil, V.; Sharma, N. Mucoadhesive Systems in Dentistry: A Review. *Indian Journal of Dental Research* **2016**, *4*, 25-29. <https://doi.org/10.14419/ijdr.v4i2.6283>.
6. Sharma, R.; Kumar, S.; Malviya, R.; Prajapati, B.G.; Puri, D.; Limmatvapirat, S.; Sriamornsak, P. Recent advances in biopolymer-based mucoadhesive drug delivery systems for oral application. *Journal of Drug Delivery Science and Technology* **2024**, *91*, 105227. <https://doi.org/>.
7. Roy, S.; Pal, K.; Anis, A.; Pramanik, K.; Prabhakar, B. Polymers in Mucoadhesive Drug-Delivery Systems: A Brief Note. *Designed Monomers and Polymers* **2009**, *12*, 483-495. <https://doi.org/10.1163/138577209X12478283327236>.
8. Sandri, G.; Rossi, S.; Ferrari, F.; Bonferoni, M.C.; Caramella, C.M. Mucoadhesive Polymers as Enabling Excipients for Oral Mucosal Drug Delivery. In *Oral Mucosal Drug Delivery and Therapy*, Rathbone, M.J., Senel, S., Pather, I., Eds.; Springer US: Boston, MA, 2015; pp. 53-88.
9. McFarlane, H.E.; Döring, A.; Persson, S. The cell biology of cellulose synthesis. *Annual review of plant biology* **2014**, *65*, 69-94.
10. Jayaramudu, T.; Ko, H.-U.; Kim, H.C.; Kim, J.W.; Choi, E.S.; Kim, J. Adhesion properties of poly (ethylene oxide)-lignin blend for nanocellulose composites. *Composites Part B: Engineering* **2019**, *156*, 43-50.
11. Kontturi, K.S.; Biegaj, K.; Mautner, A.; Woodward, R.T.; Wilson, B.P.; Johansson, L.-S.; Lee, K.-Y.; Heng, J.Y.; Bismarck, A.; Kontturi, E. Noncovalent surface modification of cellulose nanopapers by adsorption of polymers from aprotic solvents. *Langmuir* **2017**, *33*, 5707-5712.
12. Ramírez, J.A.Á.; Hoyos, C.G.; Arroyo, S.; Cerrutti, P.; Foresti, M.L. Acetylation of bacterial cellulose catalyzed by citric acid: Use of reaction conditions for tailoring the esterification extent. *Carbohydrate polymers* **2016**, *153*, 686-695.
13. Mishra, R.; Sabu, A.; Tiwari, S. Materials chemistry and the futurist eco-friendly applications of nanocellulose: status and prospect. *Journal of Saudi Chemical Society* **2018**, *22*, 949-978. <https://doi.org/>.
14. Tan, H.; Marra, K.G. Injectable, biodegradable hydrogels for tissue engineering applications. *Materials* **2010**, *3*, 1746-1767.
15. Bi, L.; Cheng, W.; Fan, H.; Pei, G. Reconstruction of goat tibial defects using an injectable tricalcium phosphate/chitosan in combination with autologous platelet-rich plasma. *Biomaterials* **2010**, *31*, 3201-3211.
16. Li, H.; Ji, Q.; Chen, X.; Sun, Y.; Xu, Q.; Deng, P.; Hu, F.; Yang, J. Accelerated bony defect healing based on chitosan thermosensitive hydrogel scaffolds embedded with chitosan nanoparticles for the delivery of BMP2 plasmid DNA. *Journal of biomedical materials research Part A* **2017**, *105*, 265-273.
17. Alimardani, Y.; Mirzakhani, E.; Ansari, F.; Pourjafar, H.; Sadeghi, N. Prospective and applications of bacterial nanocellulose in dentistry. *Cellulose* **2024**, *31*, 7819-7839. <https://doi.org/10.1007/s10570-024-06098-y>.
18. Revin, V.V.; Liyaskina, E.V.; Parchaykina, M.V.; Kuzmenko, T.P.; Kurgaeva, I.V.; Revin, V.D.; Ullah, M.W. Bacterial Cellulose-Based Polymer Nanocomposites: A Review. *Polymers* **2022**, *14*, 4670.
19. Horue, M.; Silva, J.M.; Berti, I.R.; Brandão, L.R.; Barud, H.D.S.; Castro, G.R. Bacterial Cellulose-Based Materials as Dressings for Wound Healing. *Pharmaceutics* **2023**, *15*. <https://doi.org/10.3390/pharmaceutics15020424>.
20. Shrivastav, P.; Pramanik, S.; Vaidya, G.; Abdelgawad, M.A.; Ghoneim, M.M.; Singh, A.; Abualsoud, B.M.; Amaral, L.S.; Abourehab, M.A.S. Bacterial cellulose as a potential biopolymer in biomedical applications: a state-of-the-art review. *Journal of Materials Chemistry B* **2022**, *10*, 3199-3241. <https://doi.org/10.1039/D1TB02709C>.
21. Razavi, S.; Janfaza, S.; Tasnim, N.; Gibson, D.L.; Hoorfar, M. Nanomaterial-based encapsulation for controlled gastrointestinal delivery of viable probiotic bacteria. *Nanoscale Advances* **2021**, *3*, 2699-2709. <https://doi.org/10.1039/D0NA00952K>.
22. Das, M.; Lalsangi, S.; Santra, S.; Banerjee, R. Nanocellulose as a carrier for improved drug delivery: Progresses and innovation. *Journal of Drug Delivery Science and Technology* **2024**, *97*, 105743. <https://doi.org/>.
23. Yoshino, A.; Tabuchi, M.; Uo, M.; Tatsumi, H.; Hideshima, K.; Kondo, S.; Sekine, J. Applicability of bacterial cellulose as an alternative to paper points in endodontic treatment. *Acta Biomaterialia* **2013**, *9*, 6116-6122. <https://doi.org/>.
24. Xiros, C.; Christakopoulos, P. Biotechnological potential of brewers spent grain and its recent applications. *Waste and Biomass Valorization* **2012**, *3*, 213-232.
25. Pabbathi, N.P.P.; Velidandi, A.; Pogula, S.; Gandam, P.K.; Baadhe, R.R.; Sharma, M.; Sirohi, R.; Thakur, V.K.; Gupta, V.K. Brewer's spent grains-based biorefineries: A critical review. *Fuel* **2022**, *317*, 123435. <https://doi.org/>.

26. Hindi, S.S.Z. Microcrystalline cellulose: the inexhaustible treasure for pharmaceutical industry. *Nanosci. Nanotechnol. Res* **2017**, *4*, 17-24.
27. Zhao, G.; Du, J.; Chen, W.; Pan, M.; Chen, D. Preparation and thermostability of cellulose nanocrystals and nanofibrils from two sources of biomass: rice straw and poplar wood. *Cellulose* **2019**, *26*, 8625-8643. <https://doi.org/10.1007/s10570-019-02683-8>.
28. Dima, S.-O.; Panaitescu, D.-M.; Orban, C.; Ghiurea, M.; Doncea, S.-M.; Fierascu, R.C.; Nistor, C.L.; Alexandrescu, E.; Nicolae, C.-A.; Trică, B.; et al. Bacterial Nanocellulose from Side-Streams of Kombucha Beverages Production: Preparation and Physical-Chemical Properties. *Polymers* **2017**, *9*. <https://doi.org/10.3390/polym9080374>.
29. Ahmadi Heidari, N.; Fathi, M.; Hamdami, N.; Taheri, H.; Siqueira, G.; Nyström, G. Thermally Insulating Cellulose Nanofiber Aerogels from Brewery Residues. *ACS Sustainable Chemistry & Engineering* **2023**, *11*, 10698-10708. <https://doi.org/10.1021/acssuschemeng.3c01113>.
30. Tritean, N.; Dimitriu, L.; Dima, S.-O.; Ghiurea, M.; Trică, B.; Nicolae, C.-A.; Moraru, I.; Nicolescu, A.; Cimpean, A.; Oancea, F.; et al. Bioactive Hydrogel Formulation Based on Ferulic Acid-Grafted Nano-Chitosan and Bacterial Nanocellulose Enriched with Selenium Nanoparticles from Kombucha Fermentation. *Journal of Functional Biomaterials* **2024**, *15*. <https://doi.org/10.3390/jfb15070202>.
31. Lin, Y.-J.; Shatkin, J.A.; Kong, F. Evaluating mucoadhesion properties of three types of nanocellulose in the gastrointestinal tract in vitro and ex vivo. *Carbohydrate Polymers* **2019**, *210*, 157-166. <https://doi.org/>.
32. Marrinan, H.J.; Mann, J. Infrared spectra of the crystalline modifications of cellulose. *Journal of Polymer Science* **1956**, *21*, 301-311. <https://doi.org/>.
33. Vanderhart, D.L.; Atalla, R.H. Studies of microstructure in native celluloses using solid-state C-13 NMR. *Macromolecules* **1984**, *17*, 1465-1472. <https://doi.org/10.1021/ma00138a009>.
34. Sugiyama, J.; Persson, J.; Chanzy, H. Combined infrared and electron-diffraction study of the polymorphism of native celluloses. *Macromolecules* **1991**, *24*, 2461-2466. <https://doi.org/10.1021/ma00009a050>.
35. Moraru, A.; Dima, S.-O.; Tritean, N.; Oprița, E.-I.; Prelipcean, A.-M.; Trică, B.; Oancea, A.; Moraru, I.; Constantinescu-Aruxandei, D.; Oancea, F. Bioactive-Loaded Hydrogels Based on Bacterial Nanocellulose, Chitosan, and Poloxamer for Rebalancing Vaginal Microbiota. *Pharmaceutics* **2023**, *16*. <https://doi.org/10.3390/ph16121671>.
36. Tritean, N.; Dima, S.-O.; Trică, B.; Stoica, R.; Ghiurea, M.; Moraru, I.; Cimpean, A.; Oancea, F.; Constantinescu-Aruxandei, D. Selenium-Fortified Kombucha-Pollen Beverage by In Situ Biosynthesized Selenium Nanoparticles with High Biocompatibility and Antioxidant Activity. *Antioxidants* **2023**, *12*. <https://doi.org/10.3390/antiox12091711>.
37. Avgidou, M.; Dimopoulou, M.; Mackie, A.; Rigby, N.; Ritzoulis, C.; Panayiotou, C. Physicochemical aspects of mucosa surface. *RSC Adv.* **2016**, *6*, 102634-102646. <https://doi.org/10.1039/c6ra23051b>.
38. Lim, S.; Yong, G.; Chia, C.; Man, S.; Subramanian, G.; Oh, G.; Cheong, E.; Kiryukhin, M. Mucin coated protein-polyphenol microcarriers for daidzein delivery. *Food Funct.* **2024**, *15*, 2645-2654. <https://doi.org/10.1039/d3fo03356b>.
39. Ferreira, A.; Vikulina, A.; Bowker, L.; Hunt, J.; Loughlin, M.; Puddu, V.; Volodkin, D. Nanoarchitectonics of Bactericidal Coatings Based on CaCO₃-Nanosilver Hybrids. *ACS Applied Biomaterials* **2024**, *7*, 2872-2886. <https://doi.org/10.1021/acsabm.3c01228>.
40. Tritean, N.; Dimitriu, L.; Dima, S.-O.; Stoica, R.; Trică, B.; Ghiurea, M.; Moraru, I.; Cimpean, A.; Oancea, F.; Constantinescu-Aruxandei, D. Cytocompatibility, Antimicrobial and Antioxidant Activity of a Mucoadhesive Biopolymeric Hydrogel Embedding Selenium Nanoparticles Phytosynthesized by Sea Buckthorn Leaf Extract. *Pharmaceutics* **2024**, *17*. <https://doi.org/10.3390/ph17010023>.
41. Miller, A.F.; Donald, A.M. Surface and Interfacial Tension of Cellulose Suspensions. *Langmuir* **2002**, *18*, 10155-10162. <https://doi.org/10.1021/la0258300>.
42. de Amorim, J.D.P.; de Souza, K.C.; Duarte, C.R.; da Silva Duarte, I.; de Assis Sales Ribeiro, F.; Silva, G.S.; de Farias, P.M.A.; Stingl, A.; Costa, A.F.S.; Vinhas, G.M.; et al. Plant and bacterial nanocellulose: production, properties and applications in medicine, food, cosmetics, electronics and engineering. A review. *Environmental Chemistry Letters* **2020**, *18*, 851-869. <https://doi.org/10.1007/s10311-020-00989-9>.
43. Fazilati, M.; Ingelsten, S.; Wojno, S.; Nypelo, T.; Kadar, R. Thixotropy of cellulose nanocrystal suspensions. *J. Rheol.* **2021**, *65*, 1035-1052. <https://doi.org/10.1122/8.0000281>.
44. Moberg, T.; Sahlin, K.; Yao, K.; Geng, S.Y.; Westman, G.; Zhou, Q.; Oksman, K.; Rigdahl, M. Rheological properties of nanocellulose suspensions: effects of fibril/particle dimensions and surface characteristics. *Cellulose* **2017**, *24*, 2499-2510. <https://doi.org/10.1007/s10570-017-1283-0>.
45. Miyamoto, H.; Rein, D.M.; Ueda, K.; Yamane, C.; Cohen, Y. Molecular dynamics simulation of cellulose-coated oil-in-water emulsions. *Cellulose* **2017**, *24*, 2699-2711. <https://doi.org/10.1007/s10570-017-1290-1>.
46. Biermann, O.; Hädicke, E.; Koltzenburg, S.; Müller-Plathe, F. Hydrophilicity and Lipophilicity of Cellulose Crystal Surfaces. *Angewandte Chemie International Edition* **2001**, *40*, 3822-3825. <https://doi.org/10.1002/anie.200100322>.

47. KocevarNared, J.; Kristl, J.; SmidKorbar, J. Comparative rheological investigation of crude gastric mucin and natural gastric mucus. *Biomaterials* **1997**, *18*, 677-681. [https://doi.org/10.1016/s0142-9612\(96\)00180-9](https://doi.org/10.1016/s0142-9612(96)00180-9).
48. Celli, J.P.; Turner, B.S.; Afdhal, N.H.; Ewoldt, R.H.; McKinley, G.H.; Bansil, R.; Erramilli, S. Rheology of gastric mucin exhibits a pH-dependent sol-gel transition. *Biomacromolecules* **2007**, *8*, 1580-1586. <https://doi.org/10.1021/bm0609691>.
49. Li, J.; Wang, X.; Chang, C.H.; Jiang, J.; Liu, Q.; Liu, X.; Liao, Y.-P.; Ma, T.; Meng, H.; Xia, T. Nanocellulose Length Determines the Differential Cytotoxic Effects and Inflammatory Responses in Macrophages and Hepatocytes. *Small* **2021**, *17*, 2102545. <https://doi.org/>.
50. Kandhola, G.; Park, S.; Lim, J.-W.; Chivers, C.; Song, Y.H.; Chung, J.H.; Kim, J.; Kim, J.-W. Nanomaterial-Based Scaffolds for Tissue Engineering Applications: A Review on Graphene, Carbon Nanotubes and Nanocellulose. *Tissue Engineering and Regenerative Medicine* **2023**, *20*, 411-433. <https://doi.org/10.1007/s13770-023-00530-3>.
51. Amarasekara, A.S.; Wang, D.; Grady, T.L. A comparison of kombucha SCOBY bacterial cellulose purification methods. *SN Applied Sciences* **2020**, *2*, 1-7.
52. Mantle, M.; Allen, A. A Colorimetric Assay for Glycoproteins Based on the Periodic Acid/Schiff Stain. *Biochemical Society Transactions* **1978**, *6*, 607-609. <https://doi.org/10.1042/bst0060607>.
53. Hejjaji, E.; Smith, A.; Morris, G. Evaluation of the mucoadhesive properties of chitosan nanoparticles prepared using different chitosan to tripolyphosphate (CS:TPP) ratios. *International Journal of Biological Macromolecules* **2018**, *120*. <https://doi.org/10.1016/j.ijbiomac.2018.09.185>.

Disclaimer/Publisher's Note: The statements, opinions and data contained in all publications are solely those of the individual author(s) and contributor(s) and not of MDPI and/or the editor(s). MDPI and/or the editor(s) disclaim responsibility for any injury to people or property resulting from any ideas, methods, instructions or products referred to in the content.